2011 50th IEEE Conference on Decision and Control and
European Control Conference (CDC-ECC)
Orlando, FL, USA, December 12-15, 2011

Probabilistic bounds for complete scanning in non-raster atomic force microscopy

Peter I. Chang and Sean B. Andersson
Department of Mechanical Engineering, Boston University, Boston, MA 02215
{itchang,sanderss}@bu.edu

***Abstract*— Non-raster methods in atomic force microscopy seek to reduce imaging time through efficient means of information acquisition. In this work we consider the local raster-scan algorithm for imaging biopolymers and other string-like samples. Through feedback control, the scheme drives the tip along the sample to ensure measurements are collected from information-rich areas. Noise in the system, however, can cause the tip to deviate from the sample and the algorithm to fail. In this paper we use a geometric analysis to derive the probability that a loss of tracking event is due to noise. This probability is expressed in terms of the user-defined scan parameters. In turn, this allows us to quantify the probability that the sample will be scanned completely.**

I. Introduction

With its ability to acquire images with sub-nanometer spatial resolution, the atomic force microscope (AFM) [1] continues to play an important role in the fields of molecular biology, materials science, nanotechnology, and more. Its resolution, ability to measure forces at the picoNewton scale, its adaptability to different environments, and its wide variety of operation modes make it a versatile instrument. Despite these advantages, however, its temporal resolution remains poor, with commercial instruments taking seconds to minutes to generate a single image.

Recent results in high-speed AFM have yielded video rate imaging in specialized instruments [2]–[4]. Approaches have included the use of alternative physical designs [5], [6], as well as the application of advanced control techniques [7], [8]. All these methods rely on a raster-scan to build the image, reducing image time by increasing the speed at which the tip can be moved while maintaining image quality.

The imaging process can also be viewed as a problem in gathering information about a spatially (and possibly temporally) varying system using a short-range (even point-like) sensor. Viewed in this light, one can begin to consider replacing the raster-scan with alternative sampling schemes to reduce the imaging time. The challenge is to do so without degrading image quality. Many samples of interest are string-like in nature, including biopolymers such as DNA, actin, and microtubulues, as well as edges, domain boundaries, and similar features. In prior work, we have designed an algorithm termed *local raster-scanning* which uses the information acquired by the AFM in real-time to steer the tip such that it remains near the sample of interest [9], [10]. By not wasting time sampling the completely uninteresting substrate, overall imaging time can be reduced by an order-of-magnitude or more, depending on the sample.

Under our scheme, the tip follows a smooth trajectory, crossing back and forth across the sample. One such path is illustrated in Fig. 1. In this image the local raster-scan trajectory is superimposed on a standard raster-scan image of a strand of DNA. Note that the algorithm does not have access to the image but only to the measurements it has acquired along the trajectory. After completing a scan, an image is generated from the data acquired. The measurements are no longer regularly spaced, however, and thus generating an image is non-trivial. In related work, we have presented a solution to this problem using a modified Kriging interpolation scheme [11].

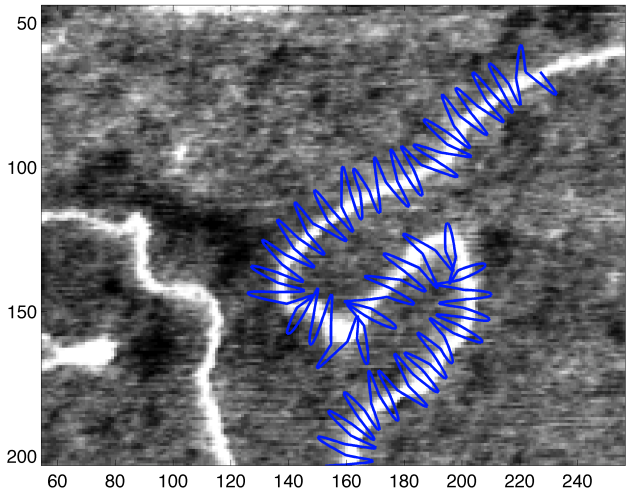

Fig. 1. Illustration of smooth local raster AFM tip trajectory scanning a DNA strand sample. The path of the tip under the local raster-scan algorithm is shown in blue, superimposed on a standard raster-scan image of the sample. Clearly, the local raster-scan approach concentrates the measurements to the vicinity of the sample.

As in any physical system, the measurements in AFM are corrupted by noise. Given the length scale of interest, such noise arises not only from the electronic components in the system but also due to thermal noise in the dynamics of the cantilever itself. Under a raster-scan, these sources simply reduce the quality of the acquired image. In the local raster-scan algorithm, however, such noise can drive the tip trajectory off of the sample, leading to loss of tracking. Of course, loss of tracking can also occur because the sample itself has ended. Because the two cannot be distinguished from the measurements, it is important to provide the user with information as to the likelihood that when the algorithm

978-1-61284-801-3/11/$26.00 ©2011 IEEE

terminates, complete scanning has occurred.

In this paper, we develop a framework to analyze this issue and then use it to derive the probability that loss of tracking was due to noise. The analysis starts from studying the geometric relationship between the designed tip trajectory and the true sample path. The uncertainties arising from the measurements are then included to account for the stochastic nature of the process.

In [12] we considered an earlier version of this problem. In that work, we considered error between the estimated and true curvatures but did not account for any difference in the error in the estimate of the heading direction of the sample. This paper takes a more comprehensive approach, accounting for both errors and introducing a probabilistic framework driven by the measurement noise.

The remainder of this paper is organized as follows. Sec. II gives a brief description of the local raster-scan algorithm and then establishes the geometric structure for the analysis to follow. This framework is used in Sec. III to derive limits on the estimation error for which detection of the underlying sample within the next scan cycle is guaranteed. In Sec. IV, these bounds are used to derive the probability of tracking the sample.

II. Tip Trajectory and Analysis Framework

We give a brief overview of the local raster-scan algorithm. Details can be found in [10].

We model the underlying sample as a planar curve $r(\cdot)$ and describe its evolution by the Frenet-Serret frame equations,

$$\begin{aligned} r'(s) &= q_1(s), \\ q_1'(s) &= \kappa(s) q_2(s), \\ q_2'(s) &= -\kappa(s) q_1(s), \end{aligned} \tag{1}$$

where the prime denotes derivative with respect to arclength s, $q_1(s)$ and $q_2(s)$ are respectively the tangent and normal to the curve at s, and $\kappa(s)$ is the curvature at s.

The tangent and normal can be expressed using a single parameter, termed the *heading direction* $\theta(s)$, according to

$$q_1(s) = \begin{bmatrix} \cos(\theta(s)) \\ \sin(\theta(s)) \end{bmatrix}, \quad q_2 = \begin{bmatrix} -\sin(\theta(s)) \\ \cos(\theta(s)) \end{bmatrix}.$$

The evolution of the curve can thus be predicted from knowledge of the curvature and heading direction by solving (1).

Under the local raster scan algorithm, the tip trajectory is given by

$$r_{tip}(s) = r(s) \pm A \sin(\omega s) q_2(s). \tag{2}$$

This path is designed to scan the tip back and forth across the sample using a smooth trajectory so as to avoid exciting unwanted dynamics in the actuators. Here A is the amplitude of the scan (analogous to image size) and ω is the scan frequency (analogous to 1/(image resolution)). These values are defined by the user prior to a scan. An illustration of a typical trajectory is given in Fig. 1.

When the tip crosses the sample, the transition between sample and substrate is detected based on the cantilever measurements (see [13] for a discussion of detection methods). Based on these detected crossing points, an estimate of the curvature and heading direction are generated. To mitigate the impact of measurement noise, these estimates are passed through a Kalman filter to produce θ_e and κ_e. Using these values, the Frenet-Serret frame equations in (1) are solved to produce the estimated curve, $r_e(\cdot)$. Note that the curvature is held constant until the next measurement update. Upon the next detected transition, the estimates are calculated again and the process repeated.

In this work, we consider the problem of loss of tracking that can occur when, due to noise, modeling error, or other factors, the true sample path diverges sufficiently far from the estimated path so that no intersection occurs. To setup the analysis, consider the geometric framework depicted in Fig. 2. Let the point of the most recent detection be labeled O and let it represent the origin of a coordinate frame. The predicted normal direction defines the negative x–axis and the predicted tangent the positive y–axis. The figure shows the relationship between the estimated and true paths. The estimated sample evolution, $r_e(\cdot)$ (dashed-dotted black line), gives rise to the tip trajectory, $r_{tip}(\cdot)$ (solid black line). As shown, the true sample, $r_t(\cdot)$ (solid red line) will in general not follow the predicted path exactly.

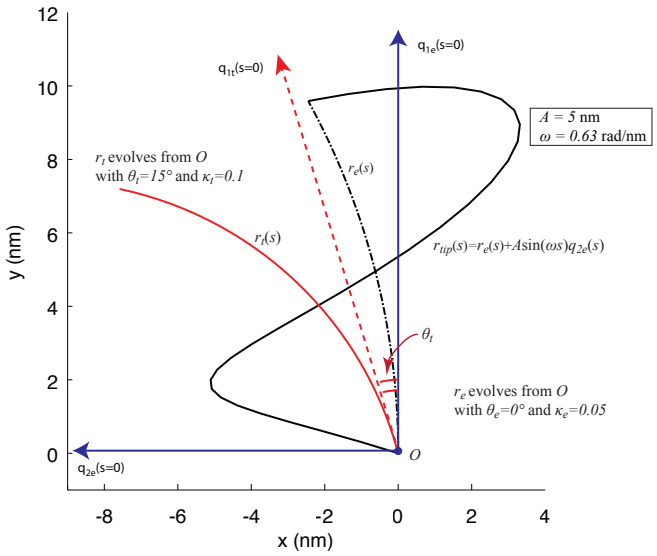

Fig. 2. Illustration of the geometric relationship between the true curve (solid red) and the predicted curve (dashed black). The tip trajectory (dashed-dotted black) is give by (2). The local frame is defined by the last intersection point (O) and the predicted Frenet-Serret frame at that point.

With this choice of coordinate system, the initial estimated heading direction is always vertical and thus we choose to measure θ_e counter-clockwise from the y–axis. The true initial heading direction may differ from zero as illustrated in the figure. Although not shown, the evolution of the predicted curve is driven by the constant curvature $\kappa_e(\cdot)$ and that of the true curve by the true curvature $\kappa_t(\cdot)$. Note that since a detection occurred at O, we assume the two curves are coincident there, ignoring the measurement error at that point.

Doing so allows us to focus on error arising from mismatch between the heading direction and curvature. As those two values are generated by taking numerical derivatives of the measured trajectory, noise in those parameters is expected to be significantly higher than in the position measurement.

We assume that the true curvature remains (approximately) constant over the span of one cycle of the tip trajectory by applying the notion of the *persistence length* of a biopolymer [14]. This length captures the stiffness of the polymer and expresses the length-scale over which a biopolymer is approximately rod-like. For example, DNA has a persistence length of approximately 50 nm [15], actin of approximately 15 μm [16], and microtubules of approximately 6 mm [17]. At distances much shorter than these, samples are typically approximated as straight lines. Here we asssume instead that the curvature does not change significantly such that over the persistence length the biopolymer is well-approximated as an arc of a circle. Since the algorithm is designed for imaging, it is reasonable to assume that the resolution is chosen well below the persistence length such that the image will have sufficient resolution to capture the details of the sample.

III. Detection Limits

As illustrated in Fig. 2, the path of the tip defined by (2) sweeps out a finite area. Clearly, only true curves within this area can be detected. The goal of this section is to establish the geometric relationship between the curves that will guarantee they will intersect in the first period of the tip trajectory.

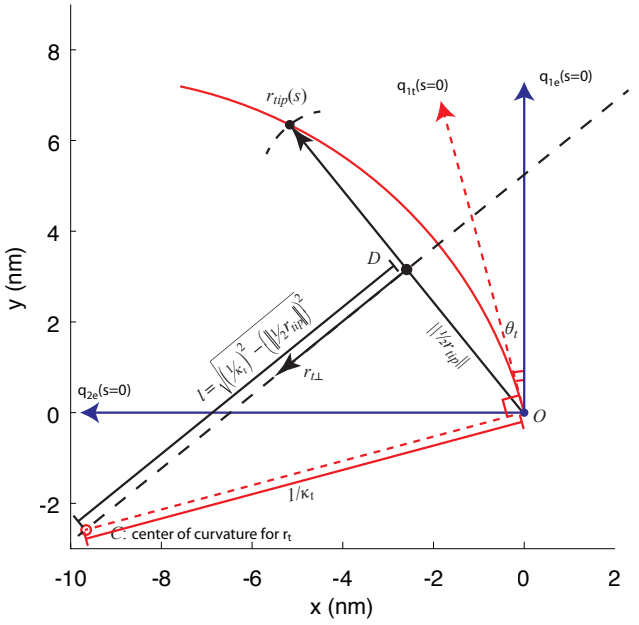

Fig. 3. Geometric relationship between the true sample path and the tip trajectory with an intersection at arclength s. Using this geometry, the center of curvature at C can be calculated and from that the corresponding initial heading direction can be calculated as in (6) and (7).

Our approach is as follows. Given a tip trajectory, we first fix a choice of true curvature. We then solve the intersection equation,

$$r_{tip}(A,\omega,r_e(\theta_e,\kappa_e),s) = r_t(\theta_t,\kappa_t) \tag{3}$$

for each value of the arclength s in $[0, 2\pi/\omega]$. The bounds on θ_t for a given κ_t are then found by determining the maximum and minimum values. In the following section, we use these results, combined with a distribution over the possible values of the true curvature and heading direction, to calculate the probability of intersection.

Consider Fig. 3. Assuming an intersection at arclength s, the true curve r_t is a circular arc spanning between the two points O and $r_{tip}(s)$. Using the known curvature κ_t, the center of curvature can be determined as follows. Let C denote this center of curvature. By definition, the distance from C to any point on the circle, including $r_{tip}(s)$ and O, is given by $1/\kappa_t$. It then follows that C falls on the normal bisector of the line $\overline{Or_{tip}}$. Denote this point as D and let $r_{tip}^{\perp}(s)$ denote a unit vector at D, pointing normal to $r_{tip}(s)$ and inward with respect to the circular arc. Then the center of curvature is given by

$$C(s) = \frac{1}{2}r_{tip}(s) + l(s)r_{tip}^{\perp}(s), \tag{4}$$

where $l(s)$ is the distance from D to C. Since $\widehat{OCD}$ is a right triangle, we have that

$$l(s) = \sqrt{\left(\frac{1}{\kappa_t}\right)^2 - \left(\frac{1}{2}||r_{tip}(s)||\right)^2}. \tag{5}$$

Let $\theta_t(0;s)$ denote the angle of the true curve intersecting the tip path at s. From the geometry in Fig. 3, this angle is given by

$$\theta_t(0;s) = \arctan\left(\frac{[C(s)]_y}{[C(s)]_x}\right) - \frac{\pi}{2}, \tag{6}$$

where $[\cdot]_{\{x,y\}}$ denotes the $\{x,y\}$ components of the vector.

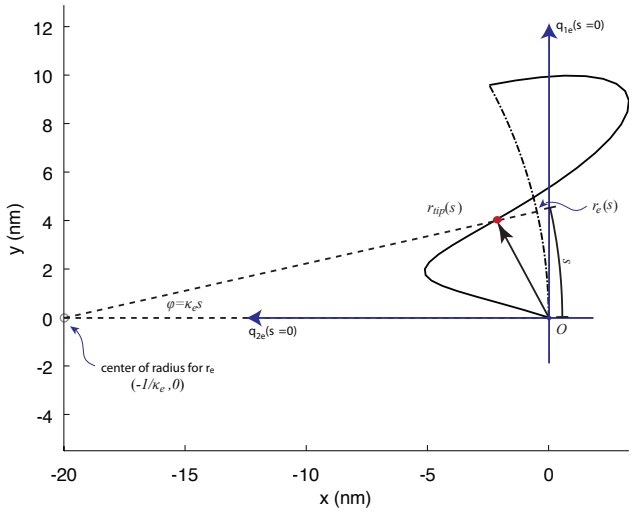

Fig. 4. Geometric relationship between the tip trajectory and the estimated path.

To relate this angle to κ_e, the path of the tip must be expressed in terms of this curvature. Consider, then, Fig.(4).

$$\theta_t(0;s) = \arctan\left(\frac{\left[\frac{1}{\kappa_e}(-1+\cos(\kappa_e s)) - A\sin(\omega s)\sin(\kappa_e s)\right] - l(s)\left[\frac{1}{\kappa_e}\sin(\kappa_e s) + A\sin(\omega s)\cos(\kappa_e s)\right]}{\left[\frac{1}{\kappa_e}\sin(\kappa_e s) + A\sin(\omega s)\cos(\kappa_e s)\right] + l(s)\left[\frac{1}{\kappa_e}(-1+\cos(\kappa_e s)) - A\sin(\omega s)\sin(\kappa_e s)\right]}\right) - \frac{\pi}{2} \tag{7}$$

By assumption, the estimated path is an arc of a circle of radius $1/\kappa_e$. By choice of the reference coordinate system, the center of curvature is located at $[-\kappa_e^{-1} \quad 0]^T$. We then immediately have that

$$r_e(s) = \frac{1}{\kappa_e}\begin{bmatrix} -1+\cos(\kappa_e s) \\ \sin(\kappa_e s) \end{bmatrix}. \tag{8}$$

Substituting (8) into (2) and using

$$q_{2e}(s) = \begin{bmatrix} -\sin(\kappa_e s) \\ \cos(\kappa_e s) \end{bmatrix},$$

yields

$$r_{tip}(s) = \frac{1}{\kappa_e}\begin{bmatrix} -1+\cos(\kappa_e s) \\ \sin(\kappa_e s) \end{bmatrix} \pm A\sin(\omega s)\begin{bmatrix} -\sin(\kappa_e s) \\ \cos(\kappa_e s) \end{bmatrix} \tag{9}$$

Finally, substituting (4), (5), and (9) into (6) yields the expression in (7) for the value of $\theta_t(0)$ that intersects the tip trajectory at s for any $s \in [0, 2\pi/\omega]$.

To determine the bounds on the detection range for a given true curvature κ_t and a given estimated path, one must find the maximum and minimum of (7) over the range $s \in [0, 2\pi/\omega]$. We therefore define

$$\begin{aligned} \theta^+ &= \max_{s\in[0,2\pi/\omega]} \theta_t(s), \\ \theta^- &= \min_{s\in[0,2\pi/\omega]} \theta_t(s). \end{aligned} \tag{10}$$

As an example, consider a scan with the parameters $A = 5$ nm and $\omega = 0.63$ rad/nm and an estimated curvature of $\kappa_e = 0.17$ nm^{-1}. The initial estimated heading direction is, by choice of the coordinate system, zero. The corresponding evolution of the estimated path of the sample as well as the tip trajectory is shown in Fig. 5.

Assume now the true curvature is $\kappa_t = 0.05$ nm^{-1}.The value of the initial true heading angle as a function of the arclength of the point of intersection, given by (7), is shown in Fig. 6. The maximum and minimum values of this curve, corresponding to θ^+ and θ^- are indicated.

Clearly the bounds on $\theta_t(0;s)$ for detection depend on the (unknown) true curvature through the length $l(s)$. This is illustrated in Fig. 7 in which this angle is plotted with respect to both s and the true curvature.

IV. Tracking Probability

The results of the previous section characterize the loss of tracking due a mismatch between the estimated parameters (θ_e, κ_e) and the true parameters (θ_t, κ_t). The result in (10) gives the limiting range on the mismatch in the heading direction such that tracking is guaranteed. This range, however, depends on full knowledge of the four parameters A, ω, κ_e, and κ_t. While the first three are known, the third is not.

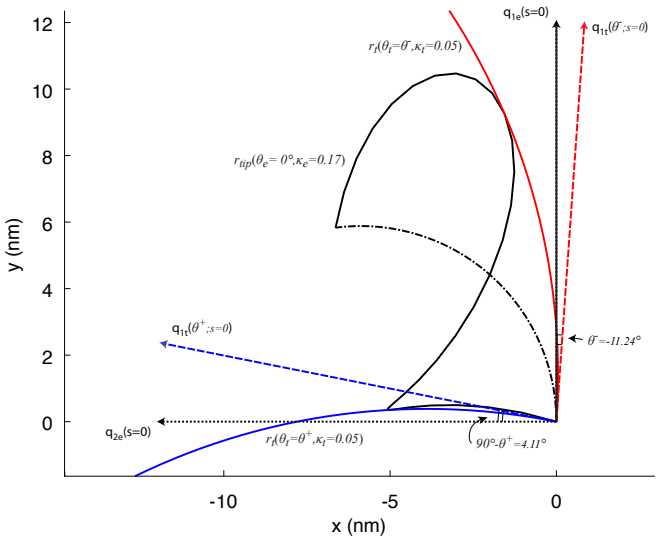

Fig. 5. Example scenario with the two limiting cases for detection. The estimated path of the sample (dash-dot black) has a curvature of $\kappa_e = 0.17$ nm^{-1} while the true curvature is $\kappa_t = 0.05$ nm^{-1}. The tip trajectory (solid black) used the parameters A=5 nm and ω = 0.63 rad/nm. The true sample paths corresponding to the limits of detection are shown in blue and red and correspond to $\theta^+ = 85.9$ rad and $\theta^- = -11.2$.

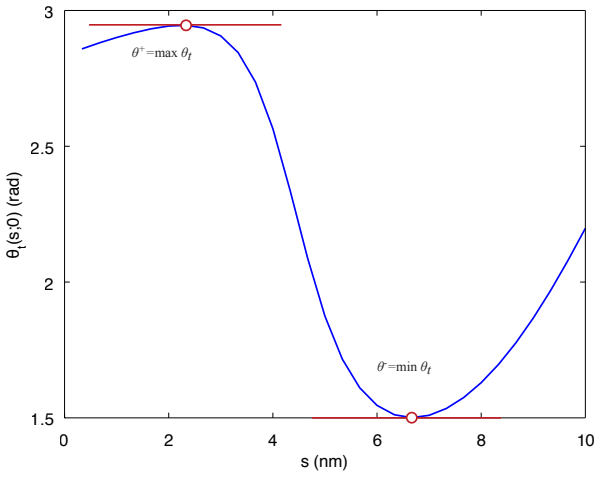

Fig. 6. Initial heading angle as a function of the arclength of the point of intersection as calculated from (7) for the example in Fig. 5.

Under the local raster-scan scheme, the estimates of the curvature and the heading direction are viewed as *noisy measurements* of the true values. These measurements are filtered using a Kalman filter. Under the assumption that the initial state and the noise processes are all Gaussian, the distributions for the curvature and heading direction are also

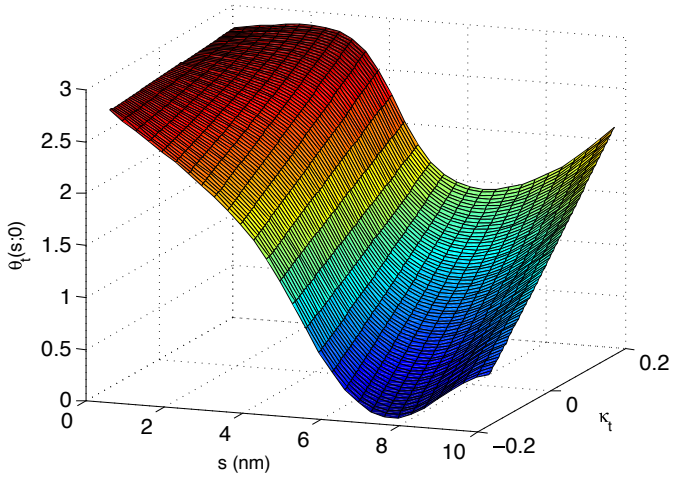

Fig. 7. Initial heading angle as a function of the arclength of the point of intersection and the true curvature, κ_t, as calculated from (7) for the example in Fig. 5.

always Gaussian. Since the Kalman filter yields the mean and covariance, the distributions are known. With this framework, we can take a probabilistic approach to the question of determining whether tracking will be lost.

Let the joint probability distribution over the true heading direction and curvature be denoted $f_{\Theta,K}(\theta_t,\kappa_t)$. As noted above, by assumption this is taken to be a joint Gaussian distribution whose statistics are updated by the Kalman filter. Since a hit will occur if and only if the true heading angle is within the bounds (θ^-,θ^+), the probability of hitting the true sample curve is given by

$$\Pr(\text{Hit}|\kappa_e) = \int_{-\infty}^{\infty}\int_{\theta^-}^{\theta^+} f_{\Theta,K}(\theta_t,\kappa_t)d\theta_t d\kappa_t. \qquad (11)$$

The true curvature is allowed to range over all values since under the Gaussian assumption the distribution has infinite support.

In practice, one may know *a priori* bounds on the curvatures which the sample can take. Such bounds can be deduced, for example, from models based on the persistence length of a biopolymer. Given such bounds, denoted as κ^+ and κ^-, the probability of a hit becomes

$$\Pr(\text{Hit}|\kappa_e) = \int_{\kappa^-}^{\kappa^+}\int_{\theta^-}^{\theta^+} f_{\Theta,K}(\theta_t,\kappa_t)d\theta_t d\kappa_t. \qquad (12)$$

In (12), the distribution should be conditioned on the known bounds of the curvature and is thus no longer Gaussian. The Kalman filter, however, only updates the mean and covariance and thus in practice the use of (12) represents an approximation.

Equations (11) and (12) provide a "one-step" probability. That is, they give the probability that a hit will occur given that a crossing of the sample was just detected. This probability can be interpreted in two ways. First, if no hit occurred in the cycle as the arclength increases from 0 to $2\pi/\omega$, (11) (or (12)) yields the probability that this was due to the sample ending as opposed to loss of tracking.

Alternatively, the scheme can be used to estimate the *a priori* probability that the entire sample will be scanned. The probability calculated by (11) or (12) is conditioned on the fact that a hit just occurred. Thus, a worst-case scenario can be determined by taking the minimum of (11) or (12) over all values of κ_e. As above, one may know bounds on the possible range of the true curvature. In that case it is reasonable to project the estimates into this range. The *a priori* probability that a successful scan will occur is thus

$$\Pr(\text{Success}) = \min_{\kappa_e\in[\kappa^-,\kappa^+]} \int_{\kappa^-}^{\kappa^+}\int_{\theta^-}^{\theta^+} f_{\Theta,K}(\theta_t,\kappa_t)d\theta_t d\kappa_t. \qquad (13)$$

Note that this probability in turn depends upon the user parameters A and ω and can provide guidance to the user in selecting the image size and resolution so as to ensure successful imaging.

V. Conclusion

In this paper, we provided an analysis framework for the local raster-scan algorithm and derived an expression for the probability that tip trajectory will intersect the sample in its next scan cycle. The result relies on knowing the probability distribution function on the curvature and heading direction of the sample and provides a means to both interpret a loss-of-tracking event and to describe the probability that a sample will be scanned given the user-defined parameters.

The probability distribution function itself is determined by the covariances of the noise parameters used in the Kalman filter. In practice, the measurements of the curvature and heading direction are generated numerically from the measurements of the crossing positions of the tip trajectory with the sample. The source of noise, then, is noise in this detection and noise in the measurements of the lateral position of the tip. These noise sources are further amplified through the numerical derivatives yielding the curvature and heading direction.

Ideally, one would like an analytical expression relating the original noise to the noise parameters used in the Kalman filter. Due to the nonlinearities of the equations, however, determining such an expression is a non-trivial task. Alternatively, one can characterize the noise through calibration experiments, that is by performing a local raster scan on samples of known geometry. The derivation of such procedures is the topic of ongoing research.

The results derived in this work are specific to the local raster-scan algorithm for high-speed imaging in AFM. The algorithm and this analysis, however, can also be applied in other contexts such as contour following and similar information acquisition problems using a point-like sensor.

Acknowledgements

This work was supported in part by a gift from Agilent Technologies and by NSF under grant no. CMMI-0845742.

REFERENCES

[1] G. Binnig, C. F. Quate, and C. Gerber, "Atomic force microscope," *Physical Review Letters*, vol. 56, no. 9, pp. 930–933, 1986.

[2] N. Kodera, D. Yamamoto, R. Ishikawa, and T. Ando, "Video imaging of walking myosin V by high-speed atomic force microscopy," *Nature*, vol. 468, no. 7320, pp. 72–76, 11 2010.

[3] G. Schitter and M. J. Rost, "Scanning probe microscopy at video-rate," *Materials Today*, vol. 11, no. 1-2, pp. 40–48, January-February 2008.

[4] G. E. Fantner, G. Schitter, J. H. Kindt, T. Ivanov, K. Ivanova, R. Patel, N. Holten-Andersen, J. Adams, P. J. Thurner, I. W. Rangelow, and P. K. Hansma, "Components for high speed atomic force microscopy," *Ultramicroscopy*, vol. 106, no. 8-9, pp. 881–887, 2006.

[5] A. J. Fleming, "Dual-stage vertical feedback for high-speed scanning probe microscopy," *IEEE Transactions on Control Systems Technology*, vol. 19, no. 1, pp. 156–165, 2010.

[6] G. Schitter, K. Astrom, B. DeMartini, P. Thurner, K. Turner, and P. Hansma, "Design and modeling of a high-speed AFM-scanner," *IEEE Transactions on Control Systems Technology*, vol. 15, no. 5, pp. 906–915, September 2007.

[7] D. R. Sahoo, A. Sebastian, and M. V. Salapaka, "Transient-signal-based sample-detection in atomic force microscopy," *Applied Physics Letters*, vol. 83, no. 26, pp. 5521–5523, 2003.

[8] Y. Yan, Q. Zou, and Z. Lin, "A control approach to high-speed probe-based nanofabrication," *Nanotechnology*, vol. 20, no. 17, p. 175301, 2009.

[9] S. B. Andersson, "Curve tracking for rapid imaging in AFM," *IEEE Transactions on Nanobioscience*, vol. 6, no. 4, pp. 354–361, 2007.

[10] P. I. Chang and S. B. Andersson, "Smooth trajectories for imaging string-like samples in AFM: A preliminary study," in *Proceedings of the American Control Conference*, 2008, pp. 3207–3212.

[11] P. Huang and S. B. Andersson, "Generating images from non-raster data," in *Proceedings of the American Control Conference*, 2011.

[12] P. I. Chang and S. B. Andersson, "Theoretical bounds on a non-raster scan method for tracking string-like samples," in *Proceedings of the American Control Conference*, 2009, pp. 2266–2271.

[13] ——, "A maximum-likelihood detection scheme for rapid imaging of string-like samples in atomic force microscopy," in *Proceedings of the IEEE Conference on Decision and Control*, 2009., pp. 8290–8295.

[14] P. Flory, *Statistical mechanics of chain molecules*. Interscience, 1969.

[15] P. J. Hagerman, "Flexibility of DNA," *Annual Review of Biophysics and Biophysical Chemistry*, vol. 17, no. 1, pp. 265–286, 2011/03/07 1988.

[16] T. Yanagida, M. Nakase, K. Nishiyama, and F. Oosawa, "Direct observation of motion of single f-actin filaments in the presence of myosin," *Nature*, vol. 307, pp. 58–60, 1984.

[17] Michey and Howard, "Rigidity of microtubules is increased by stabilizing agents," *Journal of Cell Biology*, vol. 130, pp. 909–917, 1995.